*mathematics*

MDPI

*Article*

# Mathematical Model and Analysis of Novel Bevel Gear with High Load-Capacity Based on the Geometric Elements

**Dongyu Wang [1], Luhe Zhang [1], Chao Tian [1], Jiacheng Miao [1], Laiqiang An [2], Jia Shi [3] and Bingkui Chen [1,*]**

[1] The State Key Laboratory of Mechanical Transmission for Advanced Equipment, Chongqing University, Chongqing 400000, China
[2] Institute of Materials Research, China Academy of Engineering Physics, Mianyang 621000, China
[3] Chongqing Gearbox Co., Ltd., Chongqing 400000, China
* Correspondence: bkchen@cqu.edu.cn

**Abstract:** Load-capacity has always been one of the performances that is paid much attention to in the development of bevel gear transmission applications. Consequently, the mathematical model of novel bevel gear with high load-capacity based on geometric elements is proposed in this paper, which could be applied to the aviation, aerospace and other fields. In parallel, the design principle and design method of the novel bevel gear are introduced in detail. Subsequently, the conditions for tooth surface continuity and non-interference are derived. Furthermore, the model of novel bevel gear is established. Finally, the load-bearing characteristics are analyzed, revealing that an increase in the number of contact points could significantly enhance the load capacity of the bevel gear pairs. When the load torque applied to bevel gear II is 100 Nm, the contact pressure endured by the bevel gear pair with five-point contact is decreased by 41.37% compared to the bevel gear pair with single-point contact. When the number of contact points is the same, increasing the distance between the contact points could also reduce the contact stress. This provides strong theoretical support for the application of the bevel gear based on the geometric elements.

**Keywords:** bevel gear; load capacity; running performance; transmission efficiency; geometric elements

**MSC:** 74-10



**Citation:** Wang, D.; Zhang, L.; Tian, C.; Miao, J.; An, L.; Shi, J.; Chen, B. Mathematical Model and Analysis of Novel Bevel Gear with High Load-Capacity Based on the Geometric Elements. *Mathematics* **2024**, *12*, 1373. https://doi.org/10.3390/math12091373

Academic Editor: Marco Pedroni

Received: 30 March 2024
Revised: 22 April 2024
Accepted: 25 April 2024
Published: 30 April 2024



## 1. Introduction

The bevel gear is an important fundamental mechanical component, which is widely used in various engineering fields, such as automobiles, aerospace, and marine industries [1]. In response to the increased performance demands placed on bevel gear transmission pairs, scholars have embarked on relevant research endeavors [2–5], especially in terms of the load-carrying performance of bevel gear. Kong proposed a data-oriented loaded contact pressure regulation model, in order to monitor the meshing transmission performance and improve loaded contact fatigue life [6]. Based on multi-tooth deformation compatibility, Li put forward a numerical approach to predict the load distribution of a spiral bevel gear, based on multi-tooth deformation compatibility. This approach specifically addresses the contact pressure of the spiral bevel gear [7]. Mu put forth an innovative higher-order tooth surface modification method, which could be used to reduce the vibration excitation of gear transmission [8]. Song introduced a sensitive misalignment-oriented model for regulating contact pressure, providing crucial insights into the monitoring of meshing transmission performance [9]. To achieve precise and numerically efficient tooth contact analysis, Vivet developed a penetration-based gear contact model for spiral bevel gears [10]. For both static and dynamic simulations of bevel gears, A. Pigé proposed an innovative mesh interface model. The results demonstrated that load significantly impacts the contact conditions in bevel gears [11]. Batsch presented a mathematical model

of convex-concave helical bevel gear mesh, aiming to increase the instantaneous contact area and consequently reduce the contact stress value [12]. Han proposed the nonlinear dynamic model to predict the skidding behavior [13]. Chen constructed the coupling model of mixed elastohydrodynamic transient lubrication and time-varying wear [14], and Shi analyzed the transient time-varying load to explore the thermal-pressure coupled effects under the actual operating conditions [15].

The most developed and extensively utilized tooth surface design method for spiral bevel gears is the conjugate surface meshing theory combined with local synthesis approach [16–19]. Conjugate surface meshing theory still plays a dominant role in the research of gear meshing theory. However, with the advancement of technology and to meet higher performance requirements of spiral bevel gear transmission mechanisms in industrial fields, many scholars are also proposing new meshing theory and continuously developing them in recent years. Chen proposed meshing theory based on geometric elements [20–22]. Geometric elements refer to points, curves, and surfaces, which are the three basic elements. Every combination of two of these elements forms a pair of contact relationships. Surface conjugation is one of the contact relationships, and compared to surface conjugation, curve conjugation is more diverse. Compared with general arc tooth bevel gears, bevel gears based on geometric elements could yield precise tooth surface equations and contact areas based on predetermined conjugate curves and tooth profile. Currently, such bevel gears are not suitable for applications requiring low tooth surface hardness. In order to enhance the load-carrying capacity of geometrically designed gears with soft tooth surfaces, Tan put forward a design method for bevel gears with single-point contact [23,24], and Liang developed the design method for gears based on curves elements with double contact points and three contact points [25,26]. Research by scholars has found that the gear based on the geometric elements can enhance tooth surface load-carrying capacity by increasing the number of contact points. However, the current primary research focuses on the three-point contact form, and gear designs with more than three-point contact have not yet been proposed. Therefore, the general design method for the bevel gear with multi-point contact is presented, which can be used for designing from single-point to multi-point contact.

In this paper, the general design method for the novel bevel gear pair with high load-capacity based on geometric elements is proposed, and the mathematical model is established. Subsequently, the tooth surface contact characteristics are investigated. Finally, the load-bearing characteristics of the novel bevel gear pair based on the geometric elements are analyzed.

## 2. Design Principle of Bevel Gear Based on the Geometric Elements

### *2.1. The Principle of Conjugate Curve*

The design principle of the bevel gear based on geometric elements is illustrated in Figure 1. The principle of conjugate curve is introduced in this section. The design of tooth profile and tooth surface construction are discussed in the third section.

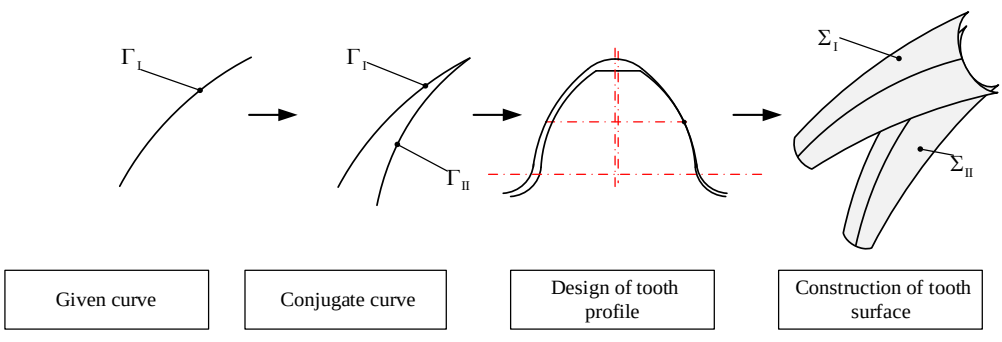


**Figure 1.** Schematic diagram of the novel bevel gear.

The conjugate curve could be characterized as a pair of smooth curves, following a prescribed motion law, which maintain continuous tangential contact along the specified direction throughout their motion, as shown in Figure 2. At each moment, curves $\Gamma_I$ and $\Gamma_{II}$ are in point contact, meaning they are tangentially touching at the contact point $H$. When the relative motion is specified, not only is curve $\Gamma_{II}$ the conjugate curve of curve $\Gamma_I$ but curve $\Gamma_I$ is also the conjugate curve of curve $\Gamma_{II}$ within a certain range.

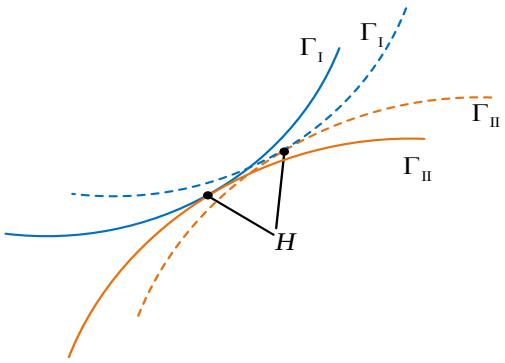


**Figure 2.** Conjugate curves.

### 2.2. Applied Coordinate System

According to the actual situation of the bevel gear drive and for the convenience of subsequent derivations, the coordinate system is established as shown in Figure 3. Coordinate systems $S_0(O_0\text{-}x_0,y_0,z_0)$ and $S_p(O_p\text{-}x_p,y_p,z_p)$ are two orthogonal right-handed coordinate systems fixed in space, where the $z_0$-axis coincides with the rotation axis of bevel gear I and the $z_p$-axis coincides with the rotation axis of bevel gear II. The shaft angle between the two revolving axles of these two bevel gears is $\psi$.

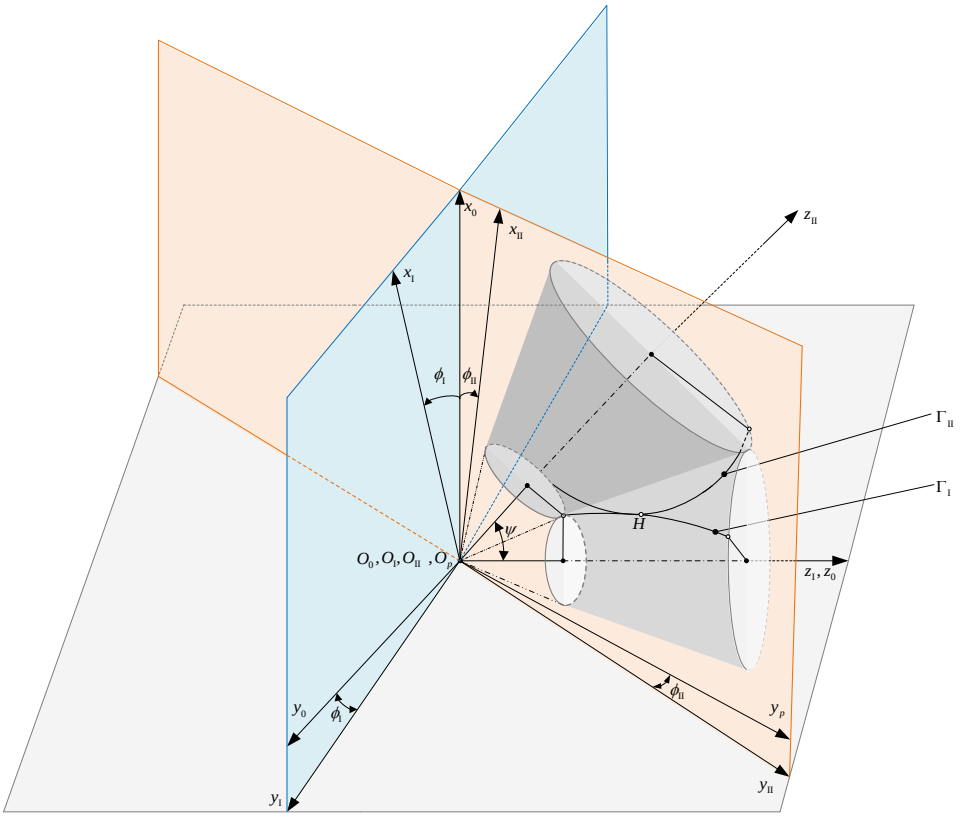


**Figure 3.** Coordinate systems.

Additionally, coordinate systems $S_I(O_I\text{-}x_I,y_I,z_I)$ and $S_{II}(O_{II}\text{-}x_{II},y_{II},z_{II})$ are respectively fixed to be right-handed orthogonal coordinate systems on bevel gear I and bevel gear II. At the initial position, they coincide respectively with coordinate systems $S_0(O_0\text{-}x_0,y_0,z_0)$ and $S_p(O_p\text{-}x_p,y_p,z_p)$. Bevel gear I rotates around the $z_0$-axis with a constant angular velocity $\boldsymbol{\omega}_I$, while bevel gear II rotates around the $z_p$-axis with a constant angular velocity $\boldsymbol{\omega}_{II}$. After a certain period of time from the initial position, coordinate systems $S_I(O_I\text{-}x_I,y_I,z_I)$ and $S_{II}(O_{II}\text{-}x_{II},y_{II},z_{II})$ move to the illustrated positions, $\phi_I$ and $\phi_{II}$ represent the angles that bevel gear I and bevel gear II have rotated through, respectively.

The transformation relationship between coordinate systems $S_0(O_0\text{-}x_0,y_0,z_0)$ and $S_I(O_I\text{-}x_I,y_I,z_I)$ is described as:

$$\boldsymbol{R}_{0I} = \begin{bmatrix} \cos\phi_I & -\sin\phi_I & 0 & 0 \\ \sin\phi_I & \cos\phi_I & 0 & 0 \\ 0 & 0 & 1 & 0 \\ 0 & 0 & 0 & 1 \end{bmatrix} \tag{1}$$

The transformation relationship between coordinate systems $S_p(O_p\text{-}x_p,y_p,z_p)$ and $S_0(O_0\text{-}x_0,y_0,z_0)$ is described as:

$$\boldsymbol{R}_{p0} = \begin{bmatrix} 1 & 0 & 0 & 0 \\ 0 & \cos\psi & -\sin\psi & 0 \\ 0 & \sin\psi & \cos\psi & 0 \\ 0 & 0 & 0 & 1 \end{bmatrix} \tag{2}$$

The transformation relationship between coordinate systems $S_{II}(O_{II}\text{-}x_{II},y_{II},z_{II})$ and $S_p(O_p\text{-}x_p,y_p,z_p)$ is described as:

$$\boldsymbol{R}_{IIp} = \begin{bmatrix} \cos\phi_{II} & -\sin\phi_{II} & 0 & 0 \\ \sin\phi_{II} & \cos\phi_{II} & 0 & 0 \\ 0 & 0 & 1 & 0 \\ 0 & 0 & 0 & 1 \end{bmatrix} \tag{3}$$

According to the principle of coordinate transformation, the transformation relationship between coordinate systems $S_{II}(O_{II}\text{-}x_{II},y_{II},z_{II})$ and $S_I(O_I\text{-}x_I,y_I,z_I)$ is obtained:

$$\boldsymbol{R}_{II\text{-}I} = \boldsymbol{R}_{IIp} \cdot \boldsymbol{R}_{p0} \cdot \boldsymbol{R}_{0I} \tag{4}$$

Substituting Equations (1)–(3) into (4), $\boldsymbol{R}_{II\text{-}I}$ is expressed as:

$$\boldsymbol{R}_{II\text{-}I} = \begin{pmatrix} \cos\phi_I\cos\phi_{II} - \cos\psi\sin\phi_I\sin\phi_{II} & -\sin\phi_I\cos\phi_{II} - \cos\psi\cos\phi_I\sin\phi_{II} & \sin\psi\sin\phi_{II} & 0 \\ \cos\phi_I\sin\phi_{II} + \cos\psi\sin\phi_I\cos\phi_{II} & -\sin\phi_I\sin\phi_{II} + \cos\psi\cos\phi_I\cos\phi_{II} & -\sin\psi\cos\phi_{II} & 0 \\ \sin\psi\sin\phi_I & \sin\psi\cos\phi_I & \cos\psi & 0 \\ 0 & 0 & 0 & 1 \end{pmatrix} \tag{5}$$

### *2.3. Meshing Equation*

#### 2.3.1. Relative Velocity

In the light of the kinematics principles, the relative velocity $\boldsymbol{v}_{I\text{-}II}$ of the meshing tooth surface points in the bevel gear pair is given by:

$$\boldsymbol{v}_{I\text{-}II} = \boldsymbol{\omega}_I \times \boldsymbol{r}_I - \boldsymbol{\omega}_{II} \times \boldsymbol{r}_{II} \tag{6}$$

where, $\boldsymbol{\omega}_I$ and $\boldsymbol{\omega}_{II}$ represent the angular velocity of bevel gear I and bevel gear II, respectively; $\boldsymbol{r}_I$ and $\boldsymbol{r}_{II}$ represent the radius vector of bevel gear I and bevel gear II, respectively.

The point $H$ in the coordinate system $S_I(O_I\text{-}x_I,y_I,z_I)$ is $H(x_I,y_I,z_I)$, and then the radius vector of bevel gear I and bevel gear II in the coordinate system $S_I(O_I\text{-}x_I,y_I,z_I)$ are described respectively:

$$\begin{cases} \boldsymbol{r}_I = x_I\boldsymbol{i}_I + y_I\boldsymbol{j}_I + z_I\boldsymbol{k}_I \\ \boldsymbol{r}_{II} = x_I\boldsymbol{i}_I + y_I\boldsymbol{j}_I + z_I\boldsymbol{k}_I \end{cases} \tag{7}$$

where, $\boldsymbol{i}_I$, $\boldsymbol{j}_I$ and $\boldsymbol{k}_I$ represent the unit vectors of the $x_I$-axes, $y_I$-axes and $z_I$-axes, respectively.

The angular velocity $\boldsymbol{\omega}_I$ of bevel gear I is obtained:

$$\boldsymbol{\omega}_I = \omega_I\boldsymbol{k}_I \tag{8}$$

where, $\omega_I$ is the module of the angular velocity $\boldsymbol{\omega}_I$.

The angular velocity $\boldsymbol{\omega}_{II}$ of bevel gear II is obtained:

$$\boldsymbol{\omega}_{II} = -\omega_{II}\sin\psi\sin\phi_I\boldsymbol{i}_I - \omega_{II}\sin\psi\cos\phi_I\boldsymbol{j}_I - \omega_{II}\cos\psi\boldsymbol{k}_I \tag{9}$$

where, $\omega_{II}$ is the module of the angular velocity $\boldsymbol{\omega}_{II}$, and $\omega_{II} = i_{II\text{-}I}\omega_I$.

Substituting Equations (6)–(8) into (5), the relative velocity $\boldsymbol{v}_{I\text{-}II}$ is expressed as:

$$\boldsymbol{v}_{I\text{-}II} = \boldsymbol{v}_{x\text{-}I\text{-}II}\boldsymbol{i}_I + \boldsymbol{v}_{y\text{-}I\text{-}II}\boldsymbol{j}_I + \boldsymbol{v}_{z\text{-}I\text{-}II}\boldsymbol{k}_I \tag{10}$$

where,

$$\begin{cases} \boldsymbol{v}_{x\text{-}I\text{-}II} = -\boldsymbol{\omega}_I(y_I + \boldsymbol{i}_{II\text{-}I}y_I\cos\psi - \boldsymbol{i}_{II\text{-}I}z_I\cos\phi_I\sin\psi) \\ \boldsymbol{v}_{y\text{-}I\text{-}II} = \boldsymbol{\omega}_I(x_I + \boldsymbol{i}_{II\text{-}I}x_I\cos\psi - \boldsymbol{i}_{II\text{-}I}z_I\sin\phi_I\sin\psi) \\ \boldsymbol{v}_{z\text{-}I\text{-}II} = \boldsymbol{i}_{II\text{-}I}\boldsymbol{\omega}_I\sin\psi(-x_I\cos\phi_I + y_I\sin\phi_I) \end{cases} \tag{11}$$

2.3.2. Meshing Equation

For the spatial curve $\Gamma_I$, an arbitrary normal vector $\boldsymbol{n}_I$ at any point on the curve can be represented (see Figure 4):

$$\boldsymbol{n}_I = \cos\alpha_I\boldsymbol{b}_I + \sin\alpha_I\boldsymbol{m}_I \tag{12}$$

where, $\boldsymbol{m}_I$ and $\boldsymbol{b}_I$ respectively represent the principal normal vector and the binormal vector of the spatial curve $\Gamma_I$, $\alpha_I$ is the angle between normal vector $\boldsymbol{n}_I$ and principal normal vector $\boldsymbol{m}_I$.

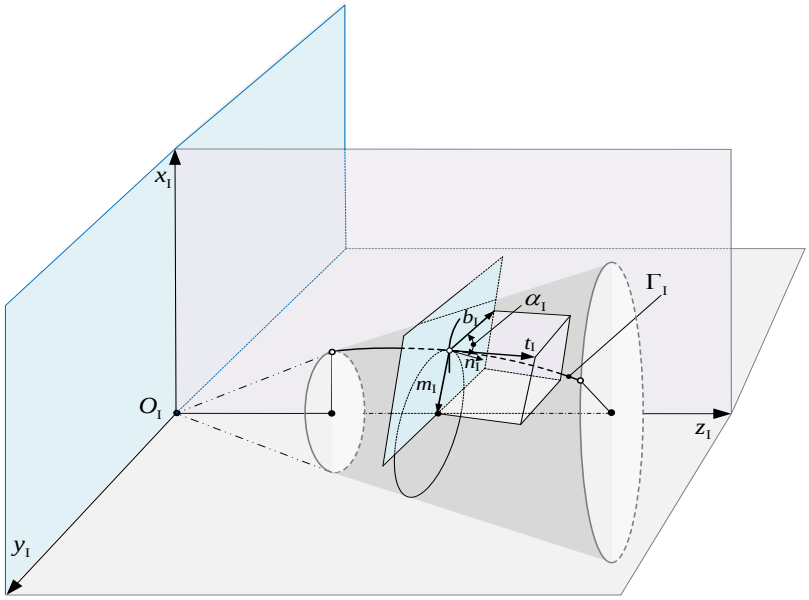


**Figure 4.** Schematic diagram of arbitrary normal vector.

In order to ensure that the given curve $\Gamma_{\mathrm{I}}$ and its conjugate curve $\Gamma_{\mathrm{II}}$ could always remain in contact throughout the motion, it is required that the projection of the relative velocity at the contact point in the normal vector direction is zero, that is, the given normal vector at the point of contact should be perpendicular to the direction of the relative velocity, which is expressed by the equation:

$$\boldsymbol{v}_{\mathrm{I\text{-}II}} \cdot \boldsymbol{n}_{\mathrm{I}} = 0 \tag{13}$$

### *2.4. Conjugate Curve*

In accordance with the definition of the conjugate curves [20], the spatial curve $\Gamma_{\mathrm{I}}$ and its conjugate curve $\Gamma_{\mathrm{II}}$ maintain point contact at every moment, and combined with Equation (13), it can be deduced that when the equation of spatial curve $\Gamma_{\mathrm{I}}$ is known, the conjugate curve $\Gamma_{\mathrm{II}}$ is obtained [22]:

$$\begin{cases} L_{\mathrm{II}}(t_{\mathrm{II}}) = \boldsymbol{M}_{\mathrm{II\text{-}I}} \cdot L_{\mathrm{I}}(t_{\mathrm{I}}) \\ \boldsymbol{v}_{\mathrm{I\text{-}II}} \cdot \boldsymbol{n}_{\mathrm{I}} = 0 \end{cases} \tag{14}$$

where, $L_{\mathrm{I}}(t_{\mathrm{I}})$ is the equation for the spatial curve $\Gamma_{\mathrm{I}}$ in coordinate system $S_{\mathrm{I}}(O_{\mathrm{I}}\text{-}x_{\mathrm{I}},y_{\mathrm{I}},z_{\mathrm{I}})$ and $L_{\mathrm{II}}(t_{\mathrm{II}})$ is the equation for the spatial curve $\Gamma_{\mathrm{II}}$ in coordinate system $S_{\mathrm{II}}(O_{\mathrm{II}}\text{-}x_{\mathrm{II}},y_{\mathrm{II}},z_{\mathrm{II}})$.

## 3. Design Method of Tooth Surfaces with High Load-Capacity

### *3.1. Principles of Design and Construction*

From the second section, the spatial curve $\Gamma_{\mathrm{I}}$ and its conjugate curve $\Gamma_{\mathrm{II}}$ are obtained. Based on this, a pair of spatial conjugate curves could be expanded into a pair of meshing surfaces which can maintain the conjugate curve meshing characteristics while achieving the transmission of motion and power, and then the model of bevel gear is established. Furthermore, it could be applied to bevel gear transmission systems.

Taking the tooth surface construction process of one of the bevel gear I as an example, the specific description is as follows: the curve $\Gamma_{s\mathrm{I}}$, called the tooth profile curve, is constructed in the normal plane of any point on the spatial curve $\Gamma_{\mathrm{I}}$. When the tooth profile curve $\Gamma_{s\mathrm{I}}$ continuously varies along the spatial curve $\Gamma_{\mathrm{I}}$, the continuous surface $\Sigma_{\mathrm{I}}$ is constructed, as shown in Figure 5.

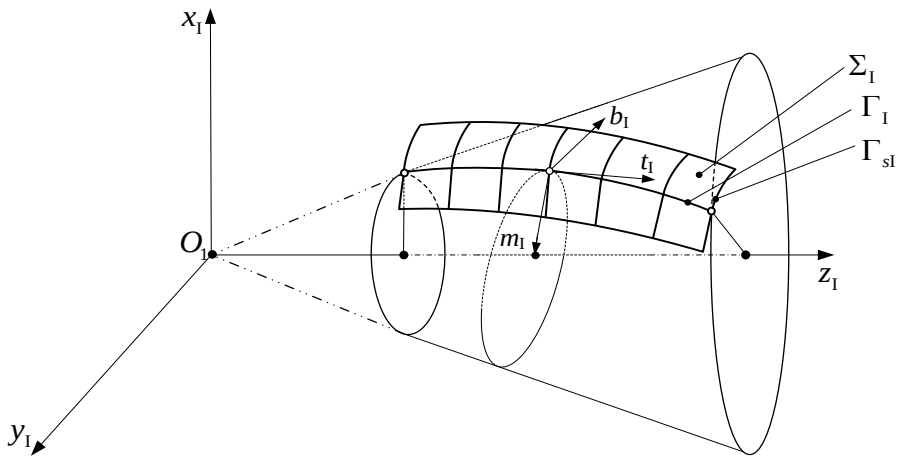


**Figure 5.** Schematic diagram of tooth surface construction.

Depend on the design requirement, it is possible to achieve multi-point contact between the tooth surfaces of bevel gear based on geometric elements by designing the tooth profile, which refers to the section curve. The general design method for the tooth profile of bevel gears with multi-point contact is proposed in this paper. The tooth profile of bevel gear I is first designed as an arc curve, and then $N$ points are selected on the arc curve as the contact points for the bevel gear pair. On the basic of these known contact points, the tooth

profile curve of bevel gear II is designed using the method of curve fitting. Subsequently, the corresponding tooth surfaces are respectively constructed according to the tooth surface construction principles.

### *3.2. Design of Tooth Profile with Multi-Point Contact*

#### 3.2.1. Tooth Profile Curve of Bevel Gear I

In accordance with the principles of tooth surface construction, the coordinate system $S_{f\mathrm{I}}$ is established at an arbitrary point $H$ on spatial curve $\Gamma_{\mathrm{I}}$ by its tangent vector $\boldsymbol{t}_{s\mathrm{I}}$, principal normal vector $\boldsymbol{m}_{s\mathrm{I}}$, and binormal vector $\boldsymbol{b}_{s\mathrm{I}}$. Subsequently, within the normal plane formed by the principal normal vector $\boldsymbol{m}_{s\mathrm{I}}$ and the binormal vector $\boldsymbol{b}_{s\mathrm{I}}$, an arc curve $\Gamma_{s\mathrm{I}}$ is constructed in the normal plane as the tooth profile curve of the bevel gear I, as shown in Figure 6. It should be noted that the principal normal vector $\boldsymbol{m}_{s\mathrm{I}}$ should be consistent with $\boldsymbol{n}_{\mathrm{I}}$ at the point $H$. The tooth profile curve of the bevel gear I in the normal plane is expressed [21]:

$$\Gamma_{s\mathrm{I}}: \begin{cases} x_{s\mathrm{I}} = \rho_{s\mathrm{I}} \cos\varphi \\ y_{s\mathrm{I}} = \rho_{s\mathrm{I}} \sin\varphi \end{cases} \tag{15}$$

where, $\rho_{s\mathrm{I}}$ is the radius of arc curve $\Gamma_{s\mathrm{I}}$ at any point, $\varphi$ is the angle between $\rho_{s\mathrm{I}}$ and $\boldsymbol{m}_{s\mathrm{I}}$, and the range of $\varphi$ is: $\varphi_{\mathrm{a}} \le \varphi \le \varphi_{\mathrm{b}}$.

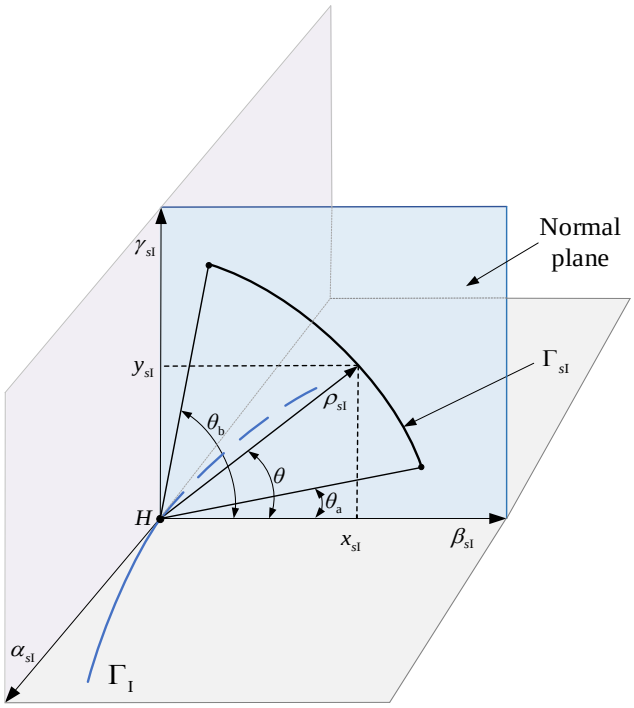


**Figure 6.** Tooth profile diagram of bevel gear I.

#### 3.2.2. Selection of Contact Points

$N$ contact points are selected on the bevel gear I arc curve, as shown in Figure 7, and then the coordinates of the $n$th contact point $A_n$ are:

$$A_n: \begin{cases} x_n = \rho_{s\mathrm{I}} \cos\varphi_n \\ y_n = \rho_{s\mathrm{I}} \sin\varphi_n \end{cases} \quad (n = 0, 1, 2, \cdots, n) \tag{16}$$

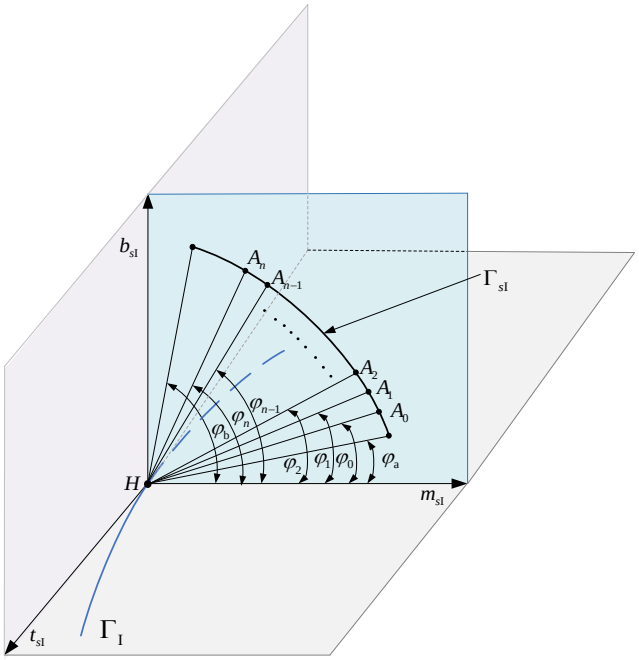


**Figure 7.** Selection of contact points.

3.2.3. Construction of Bevel Gear II Tooth Profile Curve

Considering that the tooth profile of bevel gear I is a segment of a circular curve and the selected contact point is on a circular curve, the tooth profile of bevel gear II is designed using the fitting method of the segmented quadratic trigonometric polynomial Bézier interpolation curves.

After determining the contact points, the adjacent contact points is connected with straight line in sequence and then edge vector $a_u$ is obtained:

$$a_u = A_u - A_{u-1}(u = 1, 2, \cdots, n) \tag{17}$$

Then, the tangent vector $T_u$ of the interpolation curve to be constructed at point $H_u$ is defined:

$$T_u = \begin{cases} \tau_u a_u + (1 - \tau_u) a_{u+1} (u = 1, 2, \cdots, n-1) \\ \tau_0 a_1 - (1 - \tau_0) a_2 (u = 0) \\ \tau_n a_n - (1 - \tau_n) a_{n-1} (u = n) \end{cases} \tag{18}$$

where, $\tau_u$ is the adjustment parameter of tangent vector, and the value range of $\tau_u$ is: $0 < \tau_u < 1$.

According to the definition of tangent vector $T_u$, by adjusting the tangent vector parameter $t_u$ to make $T_u$ and $T_{u+1}$ not parallel, so that the tangent line passing through point $A_u$ with $T_u$ as the tangent vector intersects with the tangent line passing through point $A_{u+1}$ with $T_{u+1}$ as the tangent vector, as shown in Figure 8. The intersection point $V_u$ is denoted:

$$V_u = A_u + \frac{|a_{u+1} \times T_{u+1}|}{|T_u \times T_{u+1}|} T_u (u = 0, 1, \cdots, n-1) \tag{19}$$

In the light of the contact point $A_u$ and the intersection $V_u$ of the tangent vectors, the four control points of the quadratic triangular Bézier curve $l_{u\text{-II}}(\xi)$ passing through the point $A_{u\text{-}1}$ and the point $A_u$ as follows:

$$\begin{cases} p_{u0} = A_{u-1} \\ p_{u1} = \eta_u A_{u-1} + (1 - \eta_u) V_{u-1} \\ p_{u2} = \chi_u A_u + (1 - \chi_u) V_{u-1} \\ p_{u3} = A_u \end{cases} (u = 1, 2, \cdots, n) \tag{20}$$

where, $\eta_u$ and $\chi_u$ are both adjustable parameters, the value range of them are respectively:

$$\begin{cases} 0 < \eta_u < 1 \\ 0 < \chi_u < 1 \end{cases} \tag{21}$$

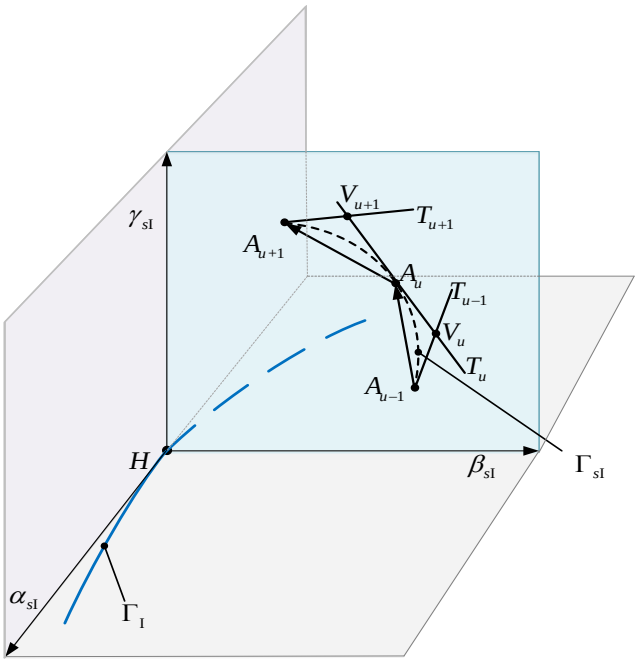


**Figure 8.** Schematic diagram of intersection point $V_u$.

In accordance with the definition of quadratic triangular Bézier curve, $l_{u\text{-II}}(\xi)$ is obtained:

$$l_{u\text{-II}}(\xi) = X_0(\xi)p_{u0} + X_1(\xi)p_{u1} + X_2(\xi)p_{u2} + X_3(\xi)p_{u3} \tag{22}$$

where, $X_0(\xi)$, $X_1(\xi)$, $X_2(\xi)$, and $X_3(\xi)$ are the primary function, they are defined:

$$\begin{cases} X_0(\xi) = (1 - \sin\xi)(1 - \lambda\sin\xi) \\ X_1(\xi) = (1 - \sin\xi)(\sin\xi + \lambda\sin\xi) \\ X_2(\xi) = (1 - \cos\xi)(\cos\xi + \lambda\cos\xi) \\ X_3(\xi) = (1 - \cos\xi)(1 - \lambda\cos\xi) \end{cases} \tag{23}$$

where, $\xi$ is the variable, the range of $\xi$ is: $0 \le \xi \le \pi/2$, and $\lambda$ is the parameter, the value range of $\lambda$ is: $-1 \le \lambda \le 1$.

### *3.3. Construction of Tooth Surface*

#### 3.3.1. Construction of Tooth Surface for Bevel Gear I

The section curve $\Gamma_{sI}$ of bevel gear I in coordinate system $S_{fI}$ is expressed:

$$\boldsymbol{r}_{sfI} = \begin{pmatrix} x_{sI} & y_{sI} & 0 & 1 \end{pmatrix}^T \tag{24}$$

Based on the principle of construction mentioned earlier, the constructed tooth surface $\Sigma_I$ is obtained, and the $\Sigma_I$ in coordinate system $S_I$ is represented:

$$\boldsymbol{r}_{\Sigma I}(\varphi, t_I) = \boldsymbol{M}_{pfI}\boldsymbol{r}_{sfI} \tag{25}$$

where,

$$\boldsymbol{M}_{pf\mathrm{I}} = \begin{pmatrix} \boldsymbol{i}_{s\mathrm{I}} \cdot \boldsymbol{\beta}_{s\mathrm{I}} & \boldsymbol{i}_{s\mathrm{I}} \cdot \boldsymbol{\gamma}_{s\mathrm{I}} & \boldsymbol{i}_{s\mathrm{I}} \cdot \boldsymbol{\alpha}_{s\mathrm{I}} & \\ \boldsymbol{j}_{s\mathrm{I}} \cdot \boldsymbol{\beta}_{s\mathrm{I}} & \boldsymbol{j}_{s\mathrm{I}} \cdot \boldsymbol{\gamma}_{s\mathrm{I}} & \boldsymbol{j}_{s\mathrm{I}} \cdot \boldsymbol{\alpha}_{s\mathrm{I}} & L_{\mathrm{I}}(t_{\mathrm{I}}) \\ \boldsymbol{k}_{s\mathrm{I}} \cdot \boldsymbol{\beta}_{s\mathrm{I}} & \boldsymbol{k}_{s\mathrm{I}} \cdot \boldsymbol{\gamma}_{s\mathrm{I}} & \boldsymbol{k}_{s\mathrm{I}} \cdot \boldsymbol{\alpha}_{s\mathrm{I}} & \\ 0 & 0 & 0 & \end{pmatrix} \tag{26}$$

3.3.2. Construction of Tooth Surface for Bevel Gear II

According to the conjugate curve principle in the second section, the conjugate curve $\Gamma_{\mathrm{II}}$ of spatial curve $\Gamma_{\mathrm{I}}$ was obtained. Then, the coordinate system $S_{f\mathrm{II}}$ is established at an arbitrary point on conjugate curve $\Gamma_{\mathrm{II}}$ by its tangent vector $\boldsymbol{\alpha}_{\mathrm{II}}$, principal normal vector $\boldsymbol{\beta}_{\mathrm{II}}$, and binormal vector $\boldsymbol{\gamma}_{\mathrm{II}}$. Unlike the section curve $\Gamma_{s1}$ of bevel gear I, the section curve $\Gamma_{s2}$ of bevel gear II is composed of a segment of interpolation curve $l_{u\text{-}\mathrm{II}}(\xi)$, and the interpolation curve $l_{u\text{-}\mathrm{II}}(\xi)$ in coordinate system $S_{f\mathrm{II}}$ is expressed:

$$\boldsymbol{r}^{g}_{sfu} = \begin{pmatrix} x^{g}_{u} & y^{g}_{u} & 0 & 1 \end{pmatrix}^{T} \tag{27}$$

Therefore, the constructed tooth surface $\Sigma^{g}_{u}$ is obtained, and the $\Sigma^{g}_{u}$ in coordinate system $S_{\mathrm{II}}$ is represented:

$$\boldsymbol{r}^{g}_{\Sigma u} = \boldsymbol{M}_{pf\mathrm{II}} \boldsymbol{r}^{g}_{sfu} \tag{28}$$

where,

$$\boldsymbol{M}_{pf\mathrm{II}} = \begin{pmatrix} \boldsymbol{i}_{s\mathrm{II}} \cdot \boldsymbol{\beta}_{s\mathrm{II}} & \boldsymbol{i}_{s\mathrm{II}} \cdot \boldsymbol{\gamma}_{s\mathrm{II}} & \boldsymbol{i}_{s\mathrm{II}} \cdot \boldsymbol{\alpha}_{s\mathrm{II}} & \\ \boldsymbol{j}_{s\mathrm{II}} \cdot \boldsymbol{\beta}_{s\mathrm{II}} & \boldsymbol{j}_{s\mathrm{II}} \cdot \boldsymbol{\gamma}_{s\mathrm{II}} & \boldsymbol{j}_{s\mathrm{II}} \cdot \boldsymbol{\alpha}_{s\mathrm{II}} & L_{\mathrm{II}}(t_{\mathrm{II}}) \\ \boldsymbol{k}_{s\mathrm{II}} \cdot \boldsymbol{\beta}_{s\mathrm{II}} & \boldsymbol{k}_{s\mathrm{II}} \cdot \boldsymbol{\gamma}_{s\mathrm{II}} & \boldsymbol{k}_{s\mathrm{II}} \cdot \boldsymbol{\alpha}_{s\mathrm{II}} & \\ 0 & 0 & 0 & \end{pmatrix} \tag{29}$$

## 4. Gear Tooth Characteristics Analysis

### *4.1. Continuity Conditions of Tooth Surface*

When constructing tooth surfaces, it is essential to ensure the continuity of the tooth surface. According to the principles of tooth surface construction, it is known that when the tooth profile curve is continuous, the generated tooth surface is also continuous. Therefore, it is necessary to derive the continuity conditions of the tooth profile curve for bevel gear II. For interpolation curves, $C^2$ continuity is generally required, meaning that the second derivative of the curve is continuous [27–29]. In order to achieve smoother interpolation curves and a smoother surface formed by these curves, this paper derives the conditions for $C^3$ continuity of the interpolation curves, ensuring that the third derivative of the interpolation curves is continuous [30].

The values of the interpolation curve $l_{u\text{-}\mathrm{II}}(\xi)$ at the starting point and endpoint of the $u$-th segment respectively are:

$$l_{u\text{-}\mathrm{II}}(0) = p_{u0} \tag{30}$$

$$l_{u\text{-}\mathrm{II}}(\frac{\pi}{2}) = p_{u3} \tag{31}$$

The values of the interpolation curve $l_{u\text{-}\mathrm{II}}(\xi)$ at the starting point and endpoint of the $(u+1)$-th segment respectively are:

$$l_{u+1\text{-}\mathrm{II}}(0) = p_{(u+1)0} \tag{32}$$

$$l_{u+1\text{-}\mathrm{II}}(\frac{\pi}{2}) = p_{(u+1)3} \tag{33}$$

It can be concluded from Equation (26) that:

$$p_{u3} = p_{(u+1)0} = A_u \tag{34}$$

The first derivative of the interpolation curve $l_{u\text{-}\mathrm{II}}(\xi)$ is obtained:

$$l_{u\text{-II}}{}'(\xi) = (1+\lambda)(p_{u1} - p_{u0})\cos\xi + ((p_{u3} - p_{u2})(1+\lambda) + 2(p_{u0}\lambda + (-p_{u1} + p_{u2})(1+\lambda) - p_{u3}\lambda)\cos\xi)\sin\xi \quad (35)$$

The second derivative of the interpolation curve $l_{u\text{-II}}(\xi)$ is obtained:

$$l_{u\text{-II}}{}''(\xi) = (p_{u3} - p_{u2})(1+\lambda)\cos\xi + 2((p_{u0} - p_{u3})\lambda + (p_{u2} - p_{u1})(1+\lambda))\cos 2\xi + (p_{u0} - p_{u1})(1+\lambda)\sin\xi \quad (36)$$

The third derivative of the interpolation curve $l_{u\text{-II}}(\xi)$ is obtained:

$$l_{u\text{-II}}{}'''(\xi) = (p_{u2} - p_{u3})(1+\lambda)\sin\xi + ((p_{u0} - p_{u1})(1+\lambda) + 8((p_{u3} - p_{u0})\lambda + (p_{u1} - p_{u2})(1+\lambda))\sin\xi)\cos\xi \quad (37)$$

To ensure the $C^1$ continuity of the interpolation curve $l_{u\text{-II}}(\xi)$, the first derivative of the interpolation curve $l_{u\text{-II}}(\xi)$ needs to be continuous, that is:

$$l_{u+1\text{-II}}{}'(0) = l_{u\text{-II}}{}'(\frac{\pi}{2}) \quad (38)$$

According to Equation (20), the first derivatives of the interpolation curve at the starting-point and endpoint values can be obtained as follows:

$$l_{u+1\text{-II}}{}'(0) = (1+\lambda_u)(p_{(u+1)1} - p_{(u+1)0}) \quad (39)$$

$$l_{u\text{-II}}{}'(\frac{\pi}{2}) = (1+\lambda_{u+1})(p_{u3} - p_{u2}) \quad (40)$$

Substituting Equations (34), (39) and (40) into (38), it could be obtained by:

$$\eta_{u+1} = 1 - (1-\chi_u)\frac{|A_u V_{u-1}|}{|A_u V_u|} \quad (41)$$

To ensure the $C^2$ continuity of the interpolation curve $l_{u\text{-II}}(\xi)$, the second derivative of the interpolation curve $l_{u\text{-II}}(\xi)$ needs to be continuous, that is:

$$l_{u+1\text{-II}}{}''(0) = l_{u\text{-II}}{}''(\frac{\pi}{2}) \quad (42)$$

$$l_{u+1\text{-II}}{}''(0) = 2\lambda_{u+1}p_{(u+1)0} - 2(1+\lambda_{u+1})p_{(u+1)1} + (1+\lambda_{u+1})p_{(u+1)2} + (1-\lambda_{u+1})p_{(u+1)3} \quad (43)$$

$$l_{u\text{-II}}{}''(\frac{\pi}{2}) = (1-\lambda_u)p_{u0} + (1+\lambda_u)p_{u1} - 2(1+\lambda_u)p_{u2} + 2\lambda_u p_{u3} \quad (44)$$

Substituting Equation (34) into (42):

$$\lambda_u = \lambda_{u+1} \quad (45)$$

The range of values for $\lambda_u$ is $0 \le \lambda_u \le 1$, and in order to achieve the continuity of the interpolation curve $l_{u\text{-II}}(\xi)$,

$$\lambda_u = \lambda_{u+1} = 1 \quad (46)$$

Substituting Equations (20), (43) and (44) into (42):

$$X_{u+1} = \frac{(3-4X_u)|V_{u-1}A_u| - \eta_u|A_{u-1}V_{u-1}| - |A_u V_u|}{|V_u A_{u+1}|} \quad (47)$$

Because the range of $X_u$ is $0 < X_{u+1} < 1$, it is deduced:

$$\frac{(3-4X_u)|V_{u-1}A_u| - |A_u V_u| - |V_u A_{u+1}|}{|V_{u-1}A_{u-1}|} < \eta_u < \frac{(3-4X_u) - |A_u V_u|}{|V_{u-1}A_{u-1}|} \quad (48)$$

The third derivative of the interpolation curve $l_{u\text{-II}}(\xi)$ needs to be continuous, that is:

$$l_{u+1\text{-II}}'''(0) = \left(p_{(u+1)0} - p_{(u+1)1}\right)(1+\lambda_{u+1}) \tag{49}$$

$$l_{u\text{-II}}'''(\frac{\pi}{2}) = (p_{u2} - p_{u3})(1+\lambda_u) \tag{50}$$

According to Equation (42), it could be concluded that:

$$p_{(u+1)1} = 2p_{u3} - p_{u2} \tag{51}$$

Substituting Equations (34) and (51) into (49):

$$l_{u+1\text{-II}}'''(0) = (p_{u2} - p_{u3})(1+\lambda_u) \tag{52}$$

Therefore, it could be deduced by:

$$l_{u+1\text{-II}}'''(0) = l_{u\text{-II}}'''(\frac{\pi}{2}) \tag{53}$$

This implies that the interpolation curve satisfies $C^3$ continuity, and when the interpolated curve satisfies $C^2$ continuity, the interpolated curve automatically satisfies $C^3$ continuity. Consequently, when the interpolated curve satisfies Equations (34), (41), (47) and (48) then the interpolated curve $l_{u\text{-II}}(\xi)$ can achieve $C^3$ continuity.

*4.2. Non-Interference Condition of Tooth Surface*

The interpolation curve is constructed after satisfying the condition of $C^3$ continuity, and then the tooth surface is constructed according to the construction principle. It is necessary to conduct interference analysis on the tooth surfaces of bevel gear I with multi-point contact and bevel gear II with multi-point contact and derive the condition that these two tooth surfaces do not interfere. According to the meshing theory of tooth surfaces, it could be determined whether there is curvature interference between two tooth surfaces based on the sign of the induced principal curvature.

If there is no curvature interference between these two tooth surfaces $\Sigma_{\mathrm{I}}$ and $\Sigma_{\mathrm{II}}$, the induced normal curvature $K_1^{\text{I-II}}$ of tooth surfaces $\Sigma_{\mathrm{I}}$ and the induced normal curvature $K_2^{\text{I-II}}$ of tooth surfaces $\Sigma_{\mathrm{I}}$ are positive values. This is the condition where there is no interference between the contact points of the bevel gear teeth, expressed as:

$$\begin{cases} K_1^{\text{I-II}} > 0 \\ K_2^{\text{I-II}} > 0 \end{cases} \tag{54}$$

According to the principles of differential geometry and tooth profile construction, the principal curvatures $K_1^{\text{I-II}}$ and $K_2^{\text{I-II}}$ could be determined:

$$K_1^{\text{I-II}} = K_1^{\mathrm{I}} - K_1^{\mathrm{II}} \tag{55}$$

$$K_2^{\text{I-II}} = K_2^{\mathrm{I}} - K_2^{\mathrm{II}} \tag{56}$$

where, $K_1^{\mathrm{I}}$ and $K_1^{\mathrm{II}}$ are the two principal curvatures of tooth profile $\Sigma_{\mathrm{I}}$; $K_2^{\mathrm{I}}$ and $K_2^{\mathrm{II}}$ are the two principal curvatures of tooth profile $\Sigma_{\mathrm{II}}$.

According to differential geometry, $K_1^{\mathrm{I}}$ and $K_2^{\mathrm{I}}$ satisfy the equation:

$$\left(E^{\mathrm{I}}G^{\mathrm{I}} - \left(F^{\mathrm{I}}\right)^2\right)\left(K_\kappa^{\mathrm{I}}\right)^2 - \left(L^{\mathrm{I}}G^{\mathrm{I}} - 2M^{\mathrm{I}}F^{\mathrm{I}} + N^{\mathrm{I}}E^{\mathrm{I}}\right)K_\kappa^{\mathrm{I}} + \left(L^{\mathrm{I}}N^{\mathrm{I}} - \left(M^{\mathrm{I}}\right)^2\right) = 0 \tag{57}$$

where, $\kappa$ represents I or II, the first and second fundamental form coefficients $E^{\mathrm{I}}$, $F^{\mathrm{I}}$, $G^{\mathrm{I}}$, $L^{\mathrm{I}}$, $M^{\mathrm{I}}$, $N^{\mathrm{I}}$ for tooth surface $\Sigma_{\mathrm{I}}$ can be separately derived [31]:

$$\begin{cases} E^{\mathrm{I}} = D(r_{\Sigma\mathrm{I}}(\varphi, t_{\mathrm{I}}), \varphi) D(r_{\Sigma\mathrm{I}}(\varphi, t_{\mathrm{I}}), \varphi) \\ F^{\mathrm{I}} = D(r_{\Sigma\mathrm{I}}(\varphi, t_{\mathrm{I}}), \varphi) D(r_{\Sigma\mathrm{I}}(\varphi, t_{\mathrm{I}}), t_{\mathrm{I}}) \\ G^{\mathrm{I}} = D(r_{\Sigma\mathrm{I}}(\varphi, t_{\mathrm{I}}), t_{\mathrm{I}}) D(r_{\Sigma\mathrm{I}}(\varphi, t_{\mathrm{I}}), t_{\mathrm{I}}) \\ L^{\mathrm{I}} = -D(r_{\Sigma\mathrm{I}}(\varphi, t_{\mathrm{I}}), \varphi) D(n_{\Sigma\mathrm{I}}(\varphi, t_{\mathrm{I}}), \varphi) \\ M^{\mathrm{I}} = -D(r_{\Sigma\mathrm{I}}(\varphi, t_{\mathrm{I}}), \varphi) D(n_{\Sigma\mathrm{I}}(\varphi, t_{\mathrm{I}}), t_{\mathrm{I}}) \\ N^{\mathrm{I}} = -D(r_{\Sigma\mathrm{I}}(\varphi, t_{\mathrm{I}}), t_{\mathrm{I}}) D(n_{\Sigma\mathrm{I}}(\varphi, t_{\mathrm{I}}), t_{\mathrm{I}}) \end{cases} \tag{58}$$

where, $D(r_{\Sigma\mathrm{I}}(\varphi,t_{\mathrm{I}}),\varphi)$ is the first derivative of $r_{\Sigma\mathrm{I}}(\varphi,t_{\mathrm{I}})$ with respect to the parameter $\varphi$, and $D(r_{\Sigma\mathrm{I}}(\varphi,t_{\mathrm{I}}),t_{\mathrm{I}})$ is the first derivative of $r_{\Sigma\mathrm{I}}(\varphi,t_{\mathrm{I}})$ with respect to the parameter $t_{\mathrm{I}}$, $D(n_{\Sigma\mathrm{I}}(\varphi,t_{\mathrm{I}}),\varphi)$ is the first derivative of unit normal vector $n_{\Sigma\mathrm{I}}(\varphi,t_{\mathrm{I}})$ of tooth surface $r_{\Sigma\mathrm{I}}$ with respect to the parameter $\varphi$, and $D(n_{\Sigma\mathrm{I}}(\varphi,t_{\mathrm{I}}),t_{\mathrm{I}})$ is the first derivative of $n_{\Sigma\mathrm{I}}(\varphi,t_{\mathrm{I}})$ with respect to the parameter $t_{\mathrm{I}}$.

The unit normal vector $n_{\Sigma\mathrm{I}}(\varphi,t_{\mathrm{I}})$ of tooth surface $r_{\Sigma\mathrm{I}}$ is obtained:

$$n_{\Sigma\mathrm{I}}(\varphi, t_{\mathrm{I}}) = \frac{D(r_{\Sigma\mathrm{I}}(\varphi, t_{\mathrm{I}}), \varphi) \times D(r_{\Sigma\mathrm{I}}(\varphi, t_{\mathrm{I}}), t_{\mathrm{I}})}{|D(r_{\Sigma\mathrm{I}}(\varphi, t_{\mathrm{I}}), \varphi) \times D(r_{\Sigma\mathrm{I}}(\varphi, t_{\mathrm{I}}), t_{\mathrm{I}})|} \tag{59}$$

For bevel gear II, it is necessary to determine the corresponding principal curvatures $K_1^{\text{I-II}}$ and $K_2^{\text{I-II}}$ of the tooth surface $r_{\Sigma u}^{g}$ formed by the interpolation curves $l_{u\text{-II}}(\xi)$ in different segments.

According to differential geometry, $K_1^{\mathrm{II}}$ and $K_2^{\mathrm{II}}$ satisfy the equation:

$$\left(E^{\mathrm{II}}G^{\mathrm{II}} - \left(F^{\mathrm{II}}\right)^2\right)\left(K_\kappa^{\mathrm{II}}\right)^2 - \left(L^{\mathrm{II}}G^{\mathrm{II}} - 2M^{\mathrm{II}}F^{\mathrm{II}} + N^{\mathrm{II}}E^{\mathrm{II}}\right)K_\kappa^{\mathrm{II}} + \left(L^{\mathrm{II}}N^{\mathrm{II}} - \left(M^{\mathrm{II}}\right)^2\right) = 0 \tag{60}$$

where, the first and second fundamental form coefficients $E^{\mathrm{II}}$, $F^{\mathrm{II}}$, $G^{\mathrm{II}}$, $L^{\mathrm{II}}$, $M^{\mathrm{II}}$, $N^{\mathrm{II}}$ for tooth surface $\Sigma_{\mathrm{II}}$ can be separately derived [31]:

$$\begin{cases} E^{\mathrm{II}} = D(r_{\Sigma u}^{g}(\xi, t_{\mathrm{II}}), \xi) D(r_{\Sigma u}^{g}(\xi, t_{\mathrm{II}}), \xi) \\ F^{\mathrm{II}} = D(r_{\Sigma u}^{g}(\xi, t_{\mathrm{II}}), \xi) D(r_{\Sigma u}^{g}(\xi, t_{\mathrm{II}}), t_{\mathrm{II}}) \\ G^{\mathrm{II}} = D(r_{\Sigma u}^{g}(\xi, t_{\mathrm{II}}), t_{\mathrm{II}}) D(r_{\Sigma u}^{g}(\xi, t_{\mathrm{II}}), t_{\mathrm{II}}) \\ L^{\mathrm{II}} = -D(r_{\Sigma u}^{g}(\xi, t_{\mathrm{II}}), \xi) D(n_{\Sigma u}^{g}(\xi, t_{\mathrm{II}}), \xi) \\ M^{\mathrm{II}} = -D(r_{\Sigma u}^{g}(\xi, t_{\mathrm{II}}), \xi) D(n_{\Sigma u}^{g}(\xi, t_{\mathrm{II}}), t_{\mathrm{II}}) \\ N^{\mathrm{II}} = -D(r_{\Sigma u}^{g}(\xi, t_{\mathrm{II}}), t_{\mathrm{II}}) D(n_{\Sigma u}^{g}(\xi, t_{\mathrm{II}}), t_{\mathrm{II}}) \end{cases} \tag{61}$$

where, $D(r_{\Sigma u}^{g}(\xi, t_{\mathrm{II}}), \xi)$ is the first derivative of $r_{\Sigma u}^{g}(\xi, t_{\mathrm{II}})$ with respect to the parameter $\xi$, and $D(r_{\Sigma u}^{g}(\xi, t_{\mathrm{II}}), t_{\mathrm{II}})$ is the first derivative of $r_{\Sigma u}^{g}(\xi, t_{\mathrm{II}})$ with respect to the parameter $t_{\mathrm{II}}$, $D(n_{\Sigma u}^{g}(\xi, t_{\mathrm{II}}), \xi)$ is the first derivative of unit normal vector $n_{\Sigma u}^{g}(\xi, t_{\mathrm{II}})$ of tooth surface $r_{\Sigma u}^{g}$ with respect to the parameter $\xi$, and $D(n_{\Sigma u}^{g}(\xi, t_{\mathrm{II}}), t_{\mathrm{II}})$ is the first derivative of $n_{\Sigma u}^{g}(\xi, t_{\mathrm{II}})$ with respect to the parameter $t_{\mathrm{II}}$.

## 5. Analysis of Load-Bearing Characteristics

### *5.1. Bevel Gear Pair Parameters*

According to the principles outlined in Sections 2 and 3, tooth surfaces with single-point, two-point, three-point, and five-point contact based on the fundamental parameters in Table 1 are constructed. Subsequently, the complete gear pairs were assembled. Figure 9 shows the model of a bevel gear pair with five-point contact.

**Table 1.** Basic parameters of bevel gear pairs.

| Parameter | Bevel Gear I | Bevel Gear II |
|---|---|---|
| Number of teeth | 8 | 24 |
| Module | 6.75 mm | |
| Pitch cone angle | 18.435 deg. | 71.565 deg. |
| Spiral angle | 35 deg. | |
| Hand of spiral | Left hand | Right hand |
| Shaft angle | 90 deg. | |
| Face width | 30 mm | |
| Outer cone distance | 83.48 mm | 250.45 mm |

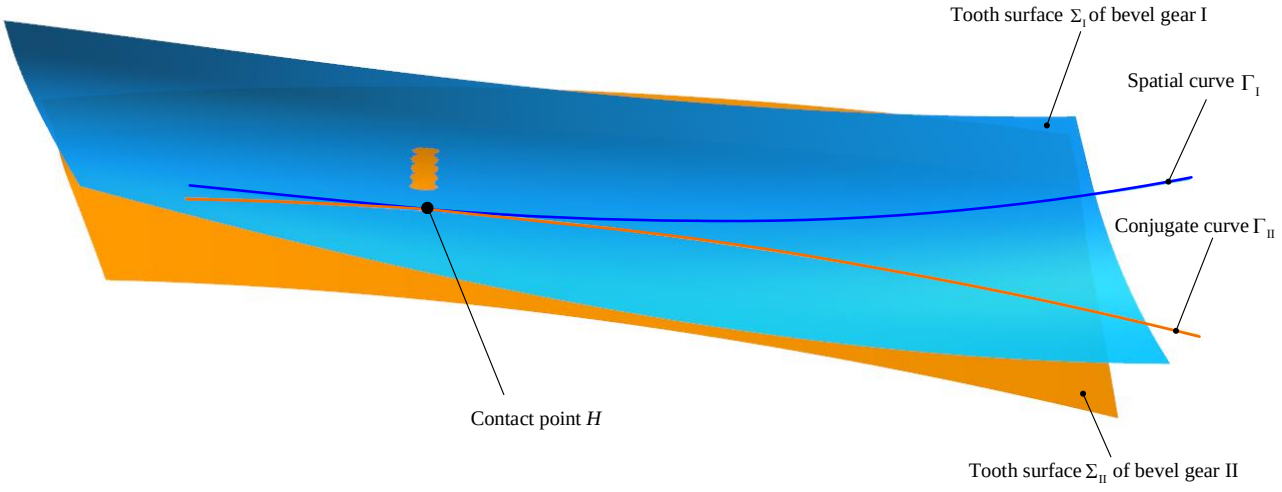


(**a**) Schematic diagram of tooth surface with five-point contact

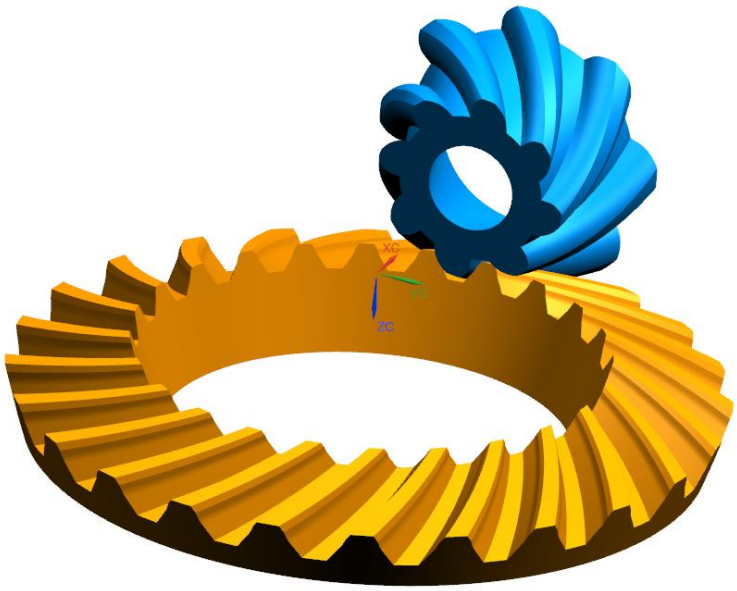

(**b**) Bevel gear model with five-point contact

**Figure 9.** Bevel gear pairs with five-point contact.

### *5.2. Influence of Meshing Points on Contact Stress*

According to the established models of bevel gear pairs with single-point, two-point, three-point, and five-point contact, contact simulations were conducted using the Abaqus software. When partitioning the mesh, C3D8I elements were employed, yielding a mesh

size of approximately 0.35. The total number of mesh elements amounted to 422,400 [24]. When selecting materials, structural steel was chosen with an elastic modulus set to 210 GPa, the Poisson's ratio is set to 0.3 and the yield strength is 850 MPa, the fracture strength is 1200 MPa [22], and the boundary conditions are set as shown in Figure 10. In Figure 10, bevel gear I and bevel gear II each have only one degree of freedom for rotation around their respective axes. An angular velocity of 3.5 rad/s around the $z_I$ axis is applied to bevel gear I, the torque of 100 Nm and 540 Nm are applied to the bevel gear II to resist the rotation of bevel gear I, respectively.

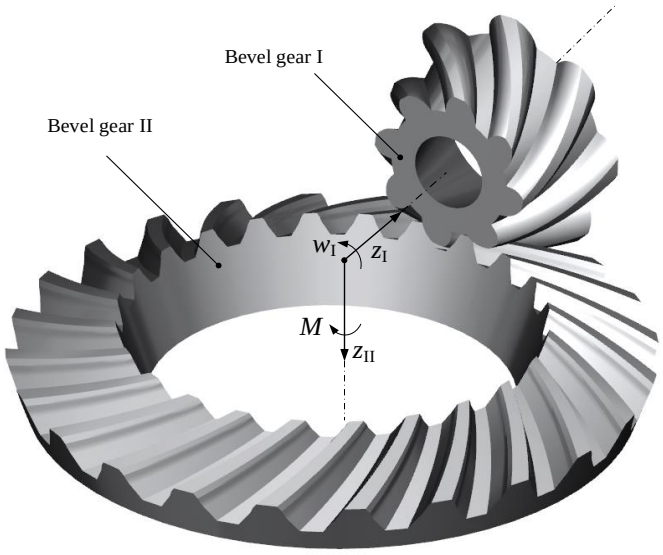


**Figure 10.** Boundary condition.

The established models of bevel gears with single-point, double-point, triple-point, and five-point contacts obtained contact pattern through simulation experiments, as shown in Figure 11. It is evident in Figure 11 that the distribution of contact points varies along the tooth height direction. The contact pattern for a single-point contact bevel gear is an ellipse close to the middle position of the tooth. For the bevel gear with double-point contact, the contact pattern consists of two ellipses. Similarly, the bevel gear with three-point contact has three ellipses, and the bevel gear with five-point contact has five ellipses. The ellipses are distributed along the tooth height direction, with the long axis in the tooth width direction. This is consistent with the contact trajectory of the literature [25,26], where there is full-width contact along the tooth width direction, and there are multiple contact points in the tooth height direction. As the bevel gear pair moves, the contact ellipses move along the tooth width direction, achieving full-width contact, as shown in Figure 12.

When the load torque of 100 Nm and 540 Nm are applied in the bevel gear II, the range from 0 degree to 22 degrees is the single tooth meshing area, the range from 22 degrees to 36 degrees is the double tooth meshing area. Subsequently, when the bevel gear I rotates from 36 degrees to 68 degrees, it corresponds to the first complete single-tooth engagement region. By repeating this process, the contact stress variation law of the bevel gear pair with multi-point contact based on the geometric elements could be obtained, as shown in Figures 13 and 14. When the number of meshing teeth is the same, the contact stress on the small gear decreases gradually from the small end to the large end. The maximum contact stress occurs on the bevel gear with single-point contact, followed by the bevel gear with double-point contact. Then the contact stress on the bevel gear with three-point contact is smaller than that on the bevel gear with double-point contact, and the lowest contact stress is observed on the bevel gear with five-point contact. Multi-point contact for bevel gear based on the geometric elements can effectively decrease the contact stress, this is consistent with the results in the literature [26].

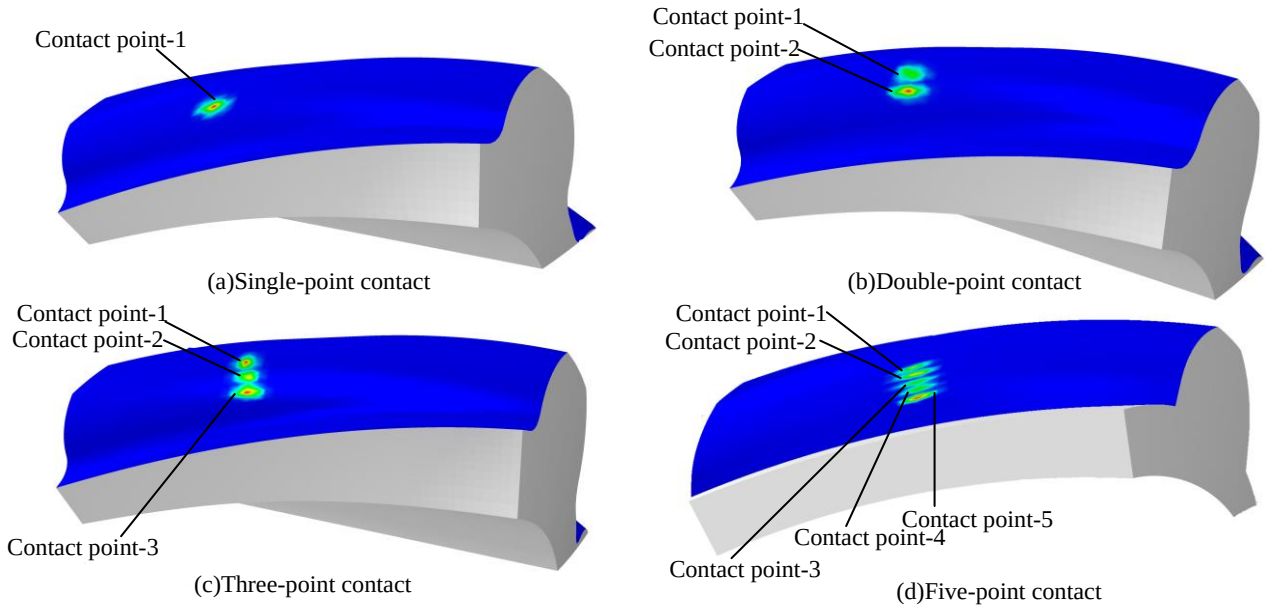


**Figure 11.** Contact pattern of bevel gear with multi-point contact.

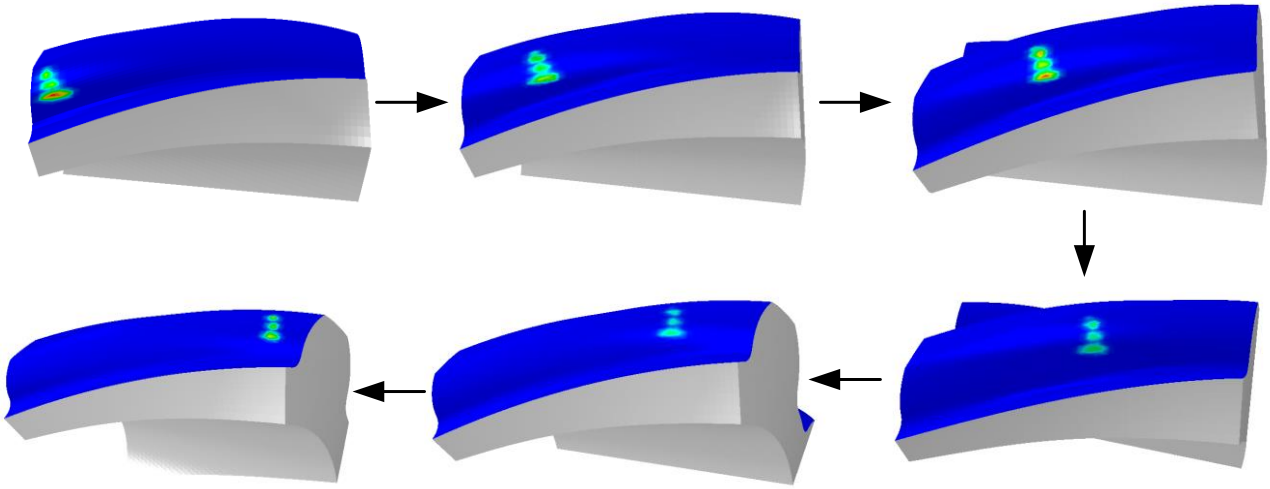

**Figure 12.** Diagram of full tooth width contact.

When the load applied in the bevel gear II is 100 Nm, the maximum contact stress on the bevel gear with single point contact in the first complete single-tooth engagement region is 742 MPa, it is 682 MPa for the bevel gear with double-point contact, it is 546 MPa for the bevel gear with three-point contact, and it is 435 MPa for the bevel gear with five-point contact. The maximum contact stress for the bevel gear with five-point contact is reduced by 41.37% compared to the maximum contact stress of the bevel gear with single-point contact, by 36.22% compared to the maximum contact stress of the bevel gear with double-point contact, and by 20.33% compared to the maximum contact stress of the bevel gear with three-point contact.

When the load applied in the bevel gear II is 540 Nm, the maximum contact stress on the bevel gear with single point contact in the first complete single-tooth engagement region is 1348 MPa. This value is close to the maximum contact pressure value reported in the literature [32]. In the literature [32], when the torque of 600 Nm is applied to bevel gear II, the maximum contact pressure for single-point contact on the mating bevel gear is 1400 MPa. The maximum contact stress is 1169 MPa for the bevel gear with double-point contact, the maximum contact stress is 1112 MPa for the bevel gear with three-point contact, and the maximum contact stress is 981 MPa for the bevel gear with five-point contact. The

maximum contact stress for the bevel gear with five-point contact is reduced by 27.23% compared to the maximum contact stress of the bevel gear with single-point contact, by 16.08% compared to the maximum contact stress of the bevel gear with double-point contact, and by 11.78% compared to the maximum contact stress of the bevel gear with three-point contact.

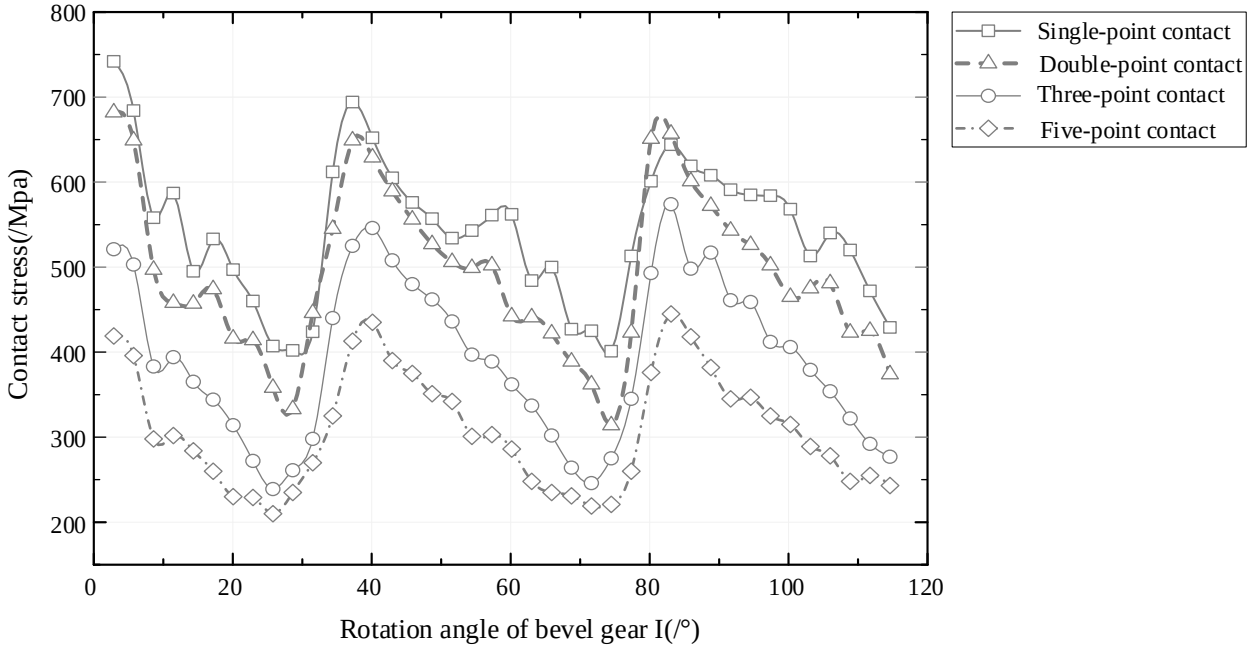


**Figure 13.** Contact stress of bevel gear pairs when loaded with 100 Nm load.

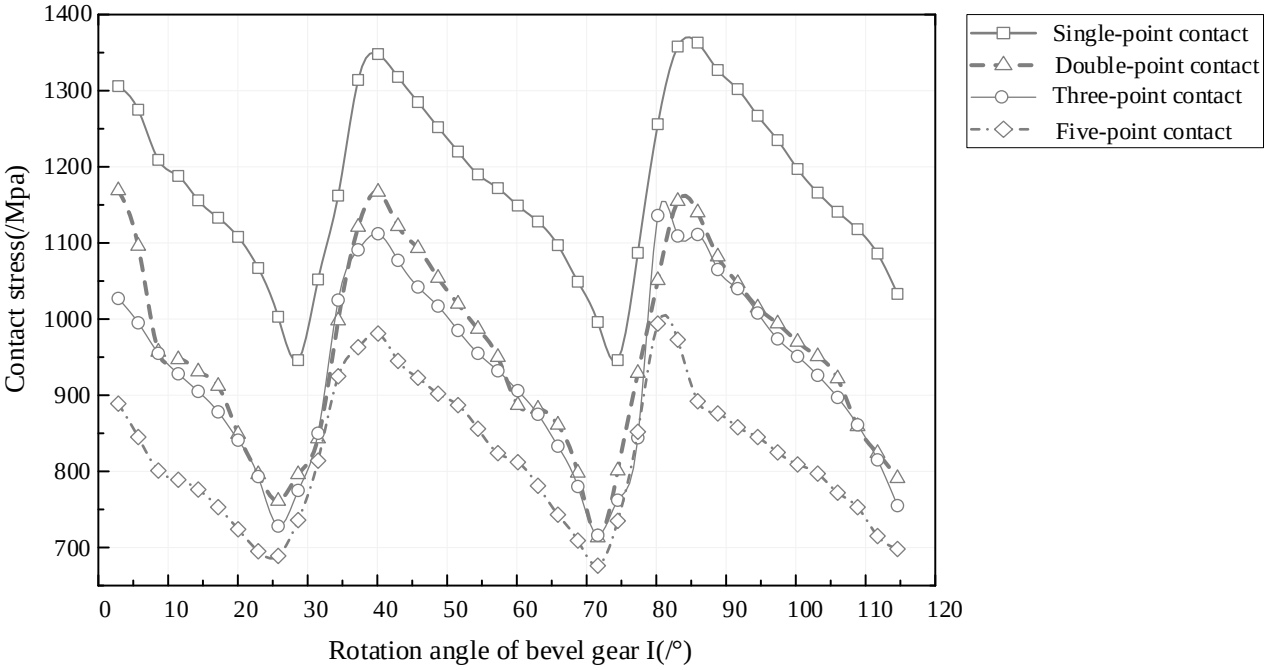


**Figure 14.** Contact stress of bevel gear pairs when loaded with 540 Nm load.

### *5.3. Influence of Distance between Contact Points on Contact Stress*

Taking the example of double-point contact bevel gear pair, the influence of the distance between contact points on the contact stress of bevel gear pairs when the number of contact points is the same is analyzed. Models of bevel gear pairs with distances of

0.005 mm, 0.007 mm, and 0.01 mm between the double contact points are respectively is established for contact analysis. The resulting contact patterns are shown in Figure 15, double contact ellipses are depicted on the tooth surface, with these two contact ellipses distributed along the tooth height direction. The difference lies in that in diagram (c), the distance between the two contact ellipses is the greatest; in diagram (b), the distance between the two contact ellipses is next; and in diagram (a), the distance between the two contact ellipses is the smallest. As the distance between the contact points decreases, the distance between the two ellipses also decreases.

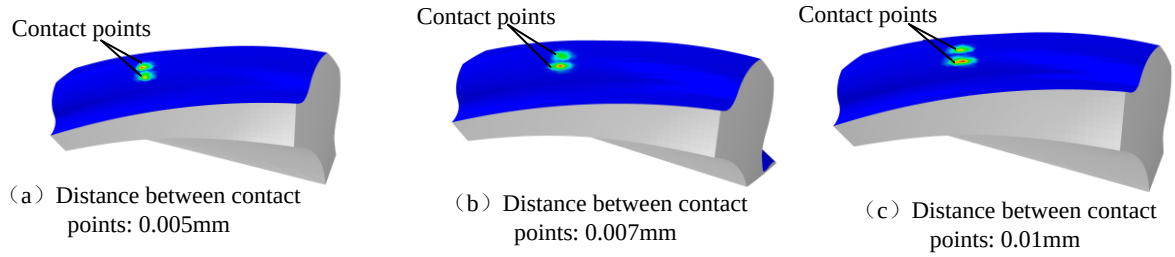


**Figure 15.** Contact patterns for bevel gears with different distances between contact points.

Figures 16 and 17 depict the variation trend of contact stress for bevel gears based on geometric elements with double-point contact from engagement to disengagement under the load of 100 Nm and 540 Nm, respectively. From Figures 16 and 17, it could be observed that the smaller the maximum non-contact distance between contact points, the lower the contact stress for the bevel gear based on geometric elements with the same number of contact points. A smaller maximum non-contact distance between contact points corresponds to lower contact stress and tends to approach contact along the tooth height line.

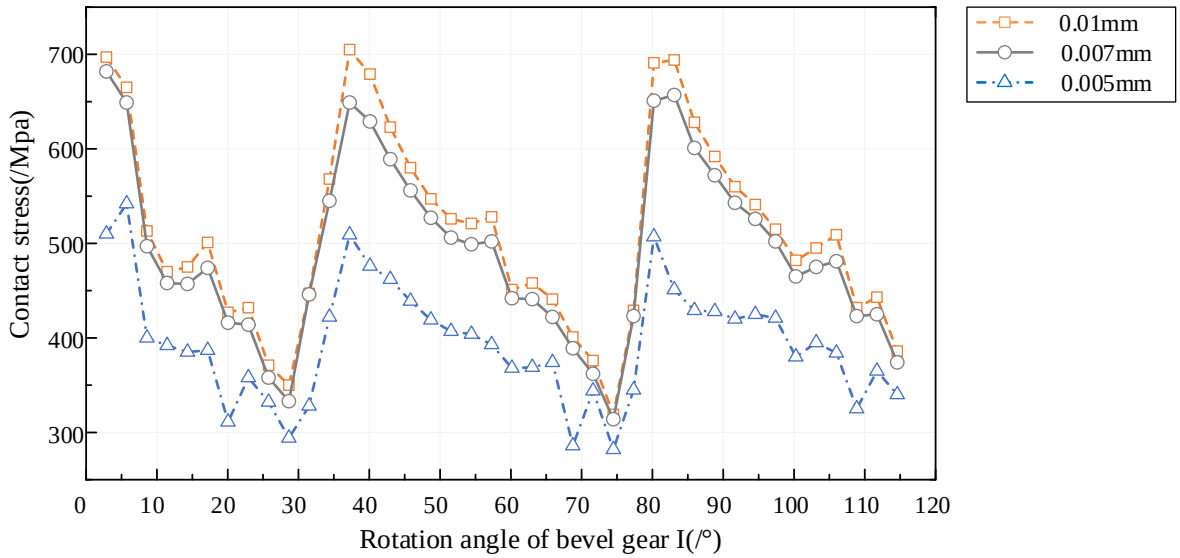


**Figure 16.** Contact stress of bevel gear pairs with double-point contact when loaded with 100 Nm load.

When the load applied in the bevel gear II is 100 Nm, the maximum contact stress on the bevel gear with the distance of 0.01 mm between the double contact points in the first complete single-tooth engagement region is 705 MPa, it is 682 MPa for the bevel gear with the distance of 0.007 mm between the double contact points, it is 542 MPa for the bevel gear with the distance of 0.005 mm between the double contact points. The maximum contact stress for the bevel gear with the distance of 0.005 mm between the double contact points is reduced by 23.21% compared to the maximum contact stress of the bevel gear

with the distance of 0.007 mm between the double contact points, by 20.52% compared to the maximum contact stress of the bevel gear with the distance of 0.01 mm between the double contact points.

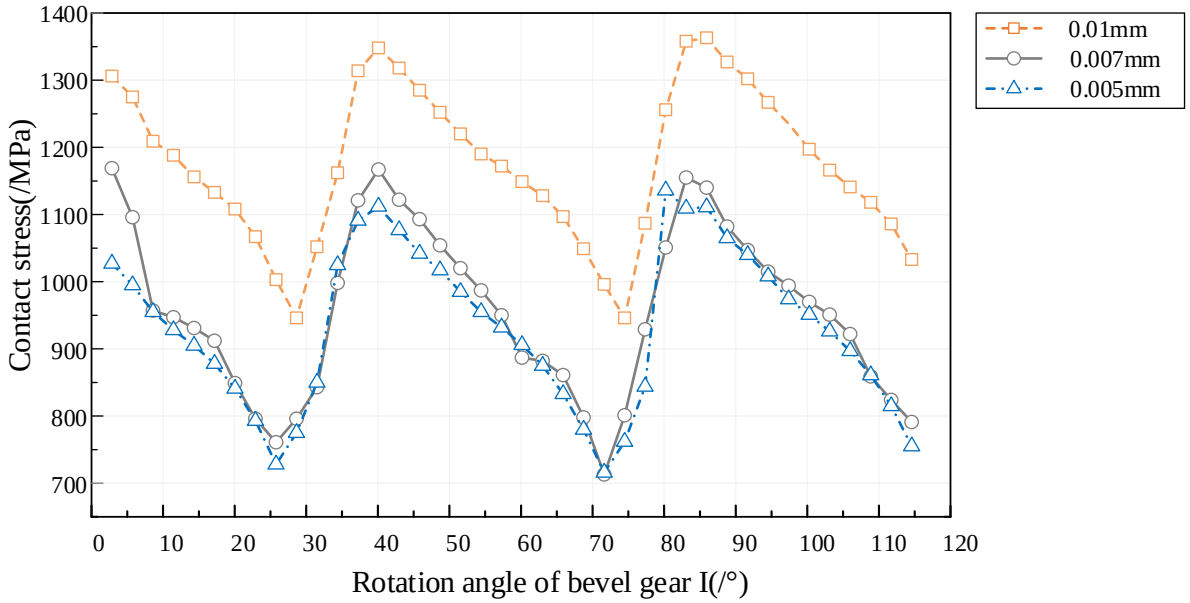


**Figure 17.** Contact stress of bevel gear pairs with double-point contact when loaded with 540 Nm load.

When the load applied in the bevel gear II is 540 Nm, the maximum contact stress on the bevel gear with the distance of 0.01 mm between the double contact points in the first complete single-tooth engagement region is 1328 MPa, it is 1169 MPa for the bevel gear with the distance of 0.007 mm between the double contact points, it is 1096 MPa for the bevel gear with the distance of 0.005 mm between the double contact points. The maximum contact stress for the bevel gear with the distance of 0.005 mm between the double contact points is reduced by 17.47% compared to the maximum contact stress of the bevel gear with the distance of 0.007 mm between the double contact points, by 6.24% compared to the maximum contact stress of the bevel gear with the distance of 0.01 mm between the double contact points.

## 6. Conclusions

In this paper, the design method of novel bevel gear with high load-capacity based on geometric elements have been proposed, and then the correlation analysis and experimental verification of the novel bevel gear were carried out. Throughout the research, there are several conclusions as follows:

(1) The design method of bevel gear with high load-capacity is put forward, the proposed novel gear enables multi-point contact in the tooth height direction, and full-tooth-width contact along the tooth width direction.

(2) The mathematical model of novel bevel gear is established, and then the analysis of gear tooth characteristics is conducted, conditions for tooth surface continuity and non-interference are also deduced.

(3) The load-bearing characteristics are analyzed, revealing that increasing the number of contact points can reduce the contact stress. For the bevel gear pair with five-point contact, the contact stress is 41.37% lower than that of a bevel gear pair with single-point contact under the torque of 100 Nm.

(4) When the number of contact points is the same, increasing the distance between the contact points can also reduce the contact stress.

(5) For the bevel gear pairs with multi-point contact based on the geometric elements, it requires higher tooth surface accuracy and still face challenges in manufacturing, which need to be further addressed.

**Author Contributions:** Conceptualization, B.C.; methodology, L.Z.; software, J.M.; formal analysis, C.T.; writing—original draft preparation, D.W.; writing—review and editing, J.S.; visualization, L.A. All authors have read and agreed to the published version of the manuscript.

**Funding:** This research was funded by the National Key R&D Program of China, grant number 2023YFB3406300.

**Data Availability Statement:** Data are contained within the article.

**Conflicts of Interest:** The authors declare no conflict of interest.

## References

1. Klingelnberg, J. (Ed.) Fields of Application for Bevel Gears. In *Bevel Gear: Fundamentals and Applications*; Springer: Berlin/Heidelberg, Germany, 2016; pp. 1–10.
2. Zhou, C.J.; Li, Z.D.; Hu, B.; Zhan, H.F.; Han, X. Analytical solution to bending and contact strength of spiral bevel gears in consideration of friction. *Int. J. Mech. Sci.* **2017**, *128*, 475–485. [CrossRef]
3. Jedlinski, L.; Jonak, J. A disassembly-free method for evaluation of spiral bevel gear assembly. *Mech. Syst. Signal Process.* **2017**, *88*, 399–412. [CrossRef]
4. Ding, H.; Tang, J.Y.; Zhong, J.; Zhou, Z.Y. A hybrid modification approach of machine-tool setting considering high tooth contact performance in spiral bevel and hypoid gears. *J. Manuf. Syst.* **2016**, *41*, 228–238. [CrossRef]
5. Yavuz, S.D.; Saribay, Z.B.; Cigeroglu, E. Nonlinear time-varying dynamic analysis of a spiral bevel geared system. *Nonlinear Dyn.* **2018**, *92*, 1901–1919. [CrossRef]
6. Kong, X.; Ding, H.; Huang, R.; Tang, J.Y. Adaptive data-driven modeling, prediction and optimal control for loaded transmission error of helicopter zero spiral bevel gear transmission system. *Mech. Mach. Theory* **2021**, *165*, 104417. [CrossRef]
7. Li, H.N.; Tang, J.Y.; Chen, S.Y.; Rong, K.B.; Ding, H.; Lu, R. Loaded contact pressure distribution prediction for spiral bevel gear. *Int. J. Mech. Sci.* **2023**, *242*, 108027. [CrossRef]
8. Mu, Y.M.; He, X.M. Design and dynamic performance analysis of high-contact-ratio spiral bevel gear based on the higher-order tooth surface modification. *Mech. Mach. Theory* **2021**, *161*, 104312. [CrossRef]
9. Song, B.Y.; Chen, J.; Zhou, Z.Y.; Rong, K.B.; Zhao, J.Y.; Ding, H. Sensitive misalignment oriented loaded contact pressure regulation model for spiral bevel gears. *Mech. Mach. Theory* **2023**, *188*, 105410. [CrossRef]
10. Vivet, M.; Tamarozzi, T.; Desmet, W.; Mundo, D. On the modelling of gear alignment errors in the tooth contact analysis of spiral bevel gears. *Mech. Mach. Theory* **2021**, *155*, 104065. [CrossRef]
11. Pigé, A.; Velex, P.; Lanquetin, R.; Cutuli, P. A model for the quasi-static and dynamic simulations of bevel gears. *Mech. Mach. Theory* **2022**, *175*, 104971.
12. Batsch, M. Mathematical model and tooth contact analysis of convexo-concave helical bevel Novikov gear mesh. *Mech. Mach. Theory* **2020**, *149*, 103842. [CrossRef]
13. Han, Q.K.; Chu, F.L. Nonlinear dynamic model for skidding behavior of angular contact ball bearings. *J. Sound Vib.* **2015**, *354*, 219–235. [CrossRef]
14. Chen, R.; Zhao, B.; He, T.; Tu, L.Y.; Xie, Z.L.; Zhong, N.; Zou, D.Q. Study on coupling transient mixed lubrication and time-varying wear of main bearing in actual operation of low-speed diesel engine. *Tribol. Int.* **2024**, *191*, 109159. [CrossRef]
15. Shi, J.H.; Zhao, B.; Tu, L.Y.; Xin, Q.; Xie, Z.L.; Zhong, N.; Lu, X.Q. Transient lubrication analysis of journal-thrust coupled bearing considering time-varying loads and thermal-pressure coupled effect. *Tribol. Int.* **2024**, *194*, 109502. [CrossRef]
16. Litvin, F.L.; Tsung, W.J.; Coy, J.J.; Heine, C. Method for generation of spiral bevel gears with conjugate gear tooth surfaces. *J. Mech. Transm. Autom. Des. Trans. Asme* **1987**, *109*, 163–170. [CrossRef]
17. Litvin, F.L.; Wang, A.G.; Handschuh, R.F. Computerized design and analysis of face-milled, uniform tooth height spiral bevel gear drives. *J. Mech. Des.* **1996**, *118*, 573–579. [CrossRef]
18. Litvin, F.L.; Fuentes, A.; Fan, Q.; Handschuh, R.F. Computerized design, simulation of meshing, and contact and stress analysis of face-milled formate generated spiral bevel gears. *Mech. Mach. Theory* **2002**, *37*, 441–459. [CrossRef]
19. Litvin, F.L.; Fuentes, A.; Hayasaka, K. Design, manufacture, stress analysis, and experimental tests of low-noise high endurance spiral bevel gears. *Mech. Mach. Theory* **2006**, *41*, 83–118. [CrossRef]
20. Chen, B.K.; Liang, D.; Li, Z.Y. A study on geometry design of spiral bevel gears based on conjugate curves. *Int. J. Precis. Eng. Manuf.* **2014**, *15*, 477–482. [CrossRef]
21. Peng, S.; Chen, B.K.; Liang, D.; Zhang, L.; Qin, S. Mathematical model and tooth contact analysis of an internal helical gear pair with selectable contact path. *Int. J. Precis. Eng. Manuf.* **2018**, *19*, 837–848. [CrossRef]
22. An, L.Q.; Zhang, L.H.; Qin, S.L.; Lan, G.; Chen, B.K. Mathematical design and computerized analysis of spiral bevel gears based on geometric elements. *Mech. Mach. Theory* **2021**, *156*, 104131. [CrossRef]

23. Tan, R.L.; Zhang, W.Q.; Guo, X.D.; Chen, B.K.; Shu, R.Z. An analytical framework of the kinematic geometry for general point-contact gears from contact path. *Proc. Inst. Mech. Eng. Part C J. Mech. Eng. Sci.* **2022**, *236*, 6363–6382. [CrossRef]
24. Tan, R.L.; Chen, B.K.; Xiang, D.; Liang, D. A study on the design and performance of epicycloid bevels of pure-rolling contact. *ASME J. Mech.* **2018**, *140*, 043301. [CrossRef]
25. Liang, D.; Li, M.; Jiang, P.; Meng, S. Optimization design and analysis of internal gear transmission with double contact points. *Proc. Inst. Mech. Eng. Part C J. Mech. Eng. Sci.* **2023**, *237*, 5788–5798. [CrossRef]
26. Liang, D.; Meng, S.; Gao, Y. Design principle and meshing analysis of internal gear drive with three contact points. *Adv. Mech. Eng.* **2022**, *14*, 16878132221081576. [CrossRef]
27. Li, J.; Song, L.; Liu, C. The cubic trigonometric automatic interpolation spline. *IEEE/CAA J. Autom. Sin.* **2018**, *5*, 1136–1141. [CrossRef]
28. Luo, Z.X. C1, C2-smooth interpolants on curved sides element. *Comput. Math. Appl.* **1998**, *35*, 125–130. [CrossRef]
29. Phung, V.M.; Nguyen, V.M.; Phan, T.H. Hermite interpolation on algebraic curves in C2. *Indag. Math.* **2019**, *30*, 874–890. [CrossRef]
30. Zhu, X.Y.; Wu, X.Q.; Chen, F.L. C~3 continuous shape-preserving piecewise quadratic triangular Bézier interpolation curves. *J. Hunan Univ. Technol.* **2012**, *25*, 25–29.
31. Chen, S.Y.; Zhang, A.Q.; Wei, J.; Lim, T.C. Nonlinear excitation and mesh characteristics model for spiral bevel gears. *Int. J. Mech. Sci.* **2023**, *257*, 108541. [CrossRef]
32. Tan, R.; Chen, B.K.; Peng, C.Y. General mathematical model of spiral bevel gears of continuous pure-rolling contact. *Proc. Inst. Mech. Eng. Part C J. Mech. Eng. Sci.* **2015**, *229*, 2810–2826. [CrossRef]